

Supporting Information of

Bendable Photodetector on Fibers Wrapped with

Flexible Ultra-Thin Single Crystalline Silicon

Nanomembranes

*Enming Song, Qinglei Guo, Gaoshan Huang, Bo Jia, Yongfeng Mei**

Department of Materials Science, Fudan University, 220 Handan Road, Shanghai 200433, China

Corresponding Author

Prof. Yongfeng Mei

*E-mail: yfm@fudan.edu.cn

- 1. Release and transfer of ultra-thin silicon nanomembranes**
- 2. Microstructure characterization of Si-NM**
- 3. Raman spectroscopy measurement**
- 4. Optoelectrical measurements**

1. Microstructure characterization of Si-NM

Many surface defects distributed throughout large Si-NMs (**Figure S1**) provide a positive path and enable HF solution etch underneath SiO₂ layer in SOI. The nano-holes (white spots) on the Si-NM surface imply two-dimension defects.

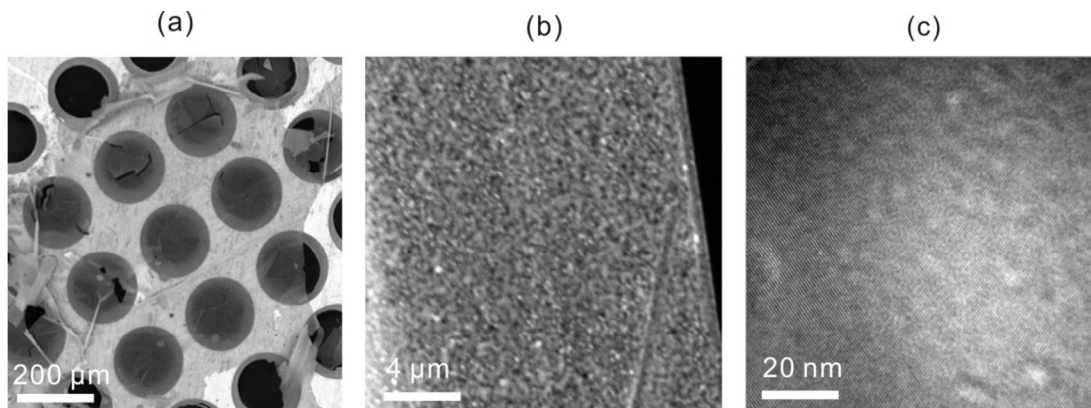


Figure S1. (a) SEM image for a Si-NM on a copper grid ready for TEM characterization and (b) a high resolution SEM image showing small defects (white color) in the Si-NMs. (c) HR-TEM image proves that nano-defects (white color) are distributed on Si-NMs.

2. Release and transfer of ultra-thin silicon nanomembranes

The original (001) silicon on insulator (SOI) wafer was scribed into 1 cm × 1 cm pieces, and then the sample was etched by 49 % HF vapor in a stable atmosphere for 30 minutes, which took away of the underneath oxide layer. Then, the Si-NM/Si sample was immersed into de-ionized water to release the top Si-NMs with assistance of liquid surface tension. The obtained Si NMs were employed to wrap optical fibers.

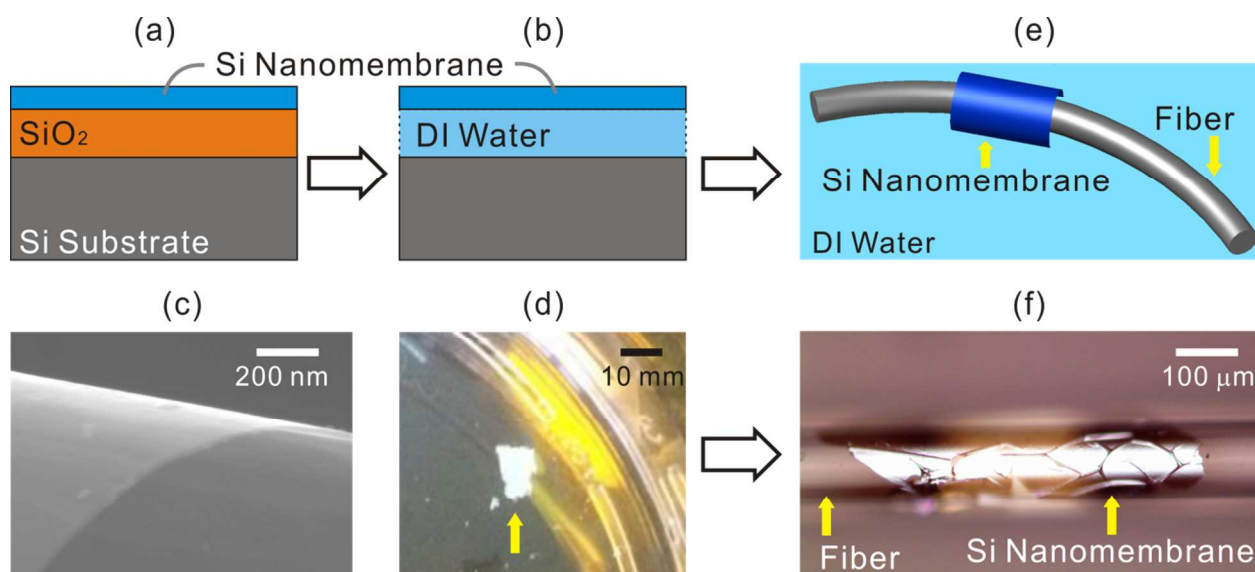


Figure S2. Schematic illustrations of (a) SOI structure and (b) Si-NMs detached from the substrate and floating on the water surface. (c) SEM image of a flexible Si-NM with a bending radius of ~ 600 nm. (d) Optical image of a released SiNM with a large area (~ 0.5 cm \times 0.5 cm) floating on the DI-water surface. (e) Sketch of an optical fiber wrapped with Si-NM and the corresponding optical microscope (OM) image. (f) Optical image of a SiNM wrapped on an optical fiber.

Specifically, a large area of Si-NM (~ 0.25 cm²) was released by HF and supported by substrate via physical-bonded interactions. Subsequently, the achieved Si-NMs on Si substrate were discreetly dipped into de-ionized water to release the NMs floating on the surface of water as schematically illustrated in **Figures S2a-b**. Then we use copper grids and optical fibers to get the NMs carefully out of water for microstructure characterization and device construction. **Figure S2c** shows a scanning electron microscope (SEM, PHILIPS XL30FEG) image of a Si-NM (~ 16.1 nm in thickness) crumpling like a piece of

paper. The optical image of the free-standing Si-NMs floating on the surface of water with an area of about $0.5\text{ cm} \times 0.5\text{ cm}$ is shown in **Figure S2d**. Subsequently, we transferred the Si-NM on a SMF as shown in **Figures S2e** (sketched) and **Figure S2f** (optical image). Good mechanical flexibility makes the ultra-thin SiNM be easily conformal wrap on the bended SMF without any visible cracks. Si-NM with several tens of nanometers in thickness displays exceptionally flexible property, with the flexural rigidity is $\sim 10^{12}$ times smaller than that of bulk silicon wafer counterpart ($200\text{ }\mu\text{m}$ in thickness).¹ In this respect, this unique mechanical property ensure the possibility for integrating Si-NMs onto flexible and curved substrates.

The bendable single mode fiber (SMF) with the core in diameter of $8\text{ }\mu\text{m}$ and the cladding layer in thickness of $125\text{ }\mu\text{m}$ is utilized as substrate to hold the flexible Si NMs. The utilized SMF is a step index single-mode industrial fiber with a numerical aperture ~ 0.15 , of which both core and cladding is consisted of SiO_2 (differently doped with Ge and B). A 20 cm long fiber was cut for subsequent preparation, a fractional section ($0.2\text{ cm} - 0.4\text{ cm}$) of which was stripped off the external organic layer in the middle of the SMF. Then the Si NMs floating on water was taken off from DI water by such fiber. The Si NMs were conformally wrapped onto the fiber. Silver paste was deposited on both ends of Si NMs as drain/ source electrodes.

3. Raman spectroscopy measurement

The Raman spectrum was accomplished by a 514 nm laser originated from a micro-Raman spectrometer system (InVia, Reinshaw) with a maximum power density of

25 $\mu\text{W}/\mu\text{m}^2$ tested by a SCIENTECH 312 Power and Energy Meter and the focal spot has a diameter of 2.5 μm on the sample surface.

Twelve groups of Si-NM Raman spectra on different curvature angles of the fiber (30° as a step, from $0\sim 360^\circ$) are recorded and displayed in **Figure S3**, where there are almost no shifts. More specifically, we started with a 20-cm straight long fiber with a Si-NM wrapped on it and then bended into various curvature angles (straight line and bended loop corresponding to 0 and 360° , respectively). The variations of Raman shifts on Si-NMs at different bending states are also less than 0.1cm^{-1} , which indicates that the residual stress in Si-NM is considerably small. The Raman peak as shown in the inset of Figure S2 of our Si-NMs is located at 519.1 cm^{-1} , which is fitted by the Gaussian curve.

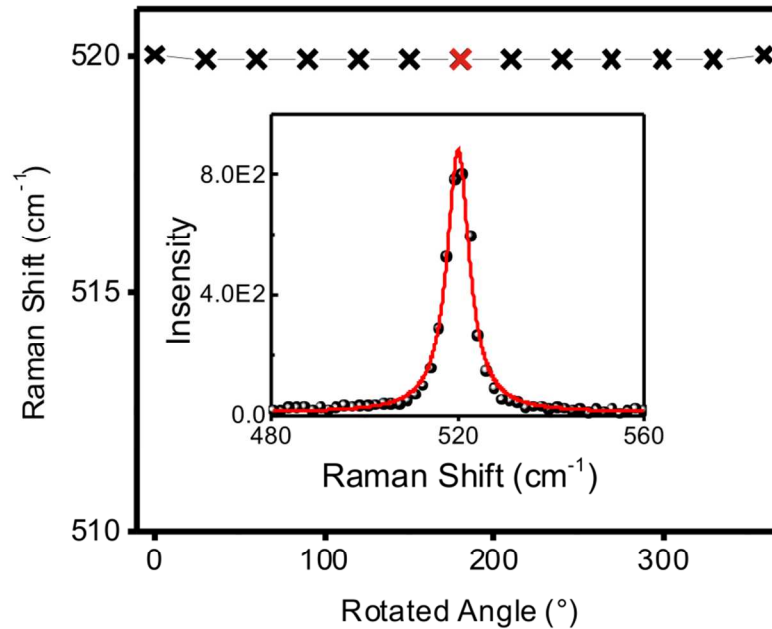


Figure S3. Raman spectra of Si-NMs on the same position along with various curvature angles of the fiber (30° as a step, from $0\sim 360^\circ$; loop shape corresponds to 360°). Inset, the experimental and fitting data of the Raman shift with a peak position of 519.1 cm^{-1} .

4. Optoelectrical measurements and band alignment theory

The Si-NM-wrapped SMF photodetector was measured by a semiconductor parameter analyzer (Keithley, SCS-4200). **Figure S4a** presents dark current versus bias (I-V) curves of Si-NMs with various bending curvatures ($0, 0.2, \text{ and } 0.5\text{ cm}^{-1}$). For the photocurrent measurement, the illumination method is realized by coupling a laser light into one end of SMF and out of the other. The light source through the SMF is with the wavelength of 633 nm and its power is 50 mW with the laser spot diameter is less than 5 mm .

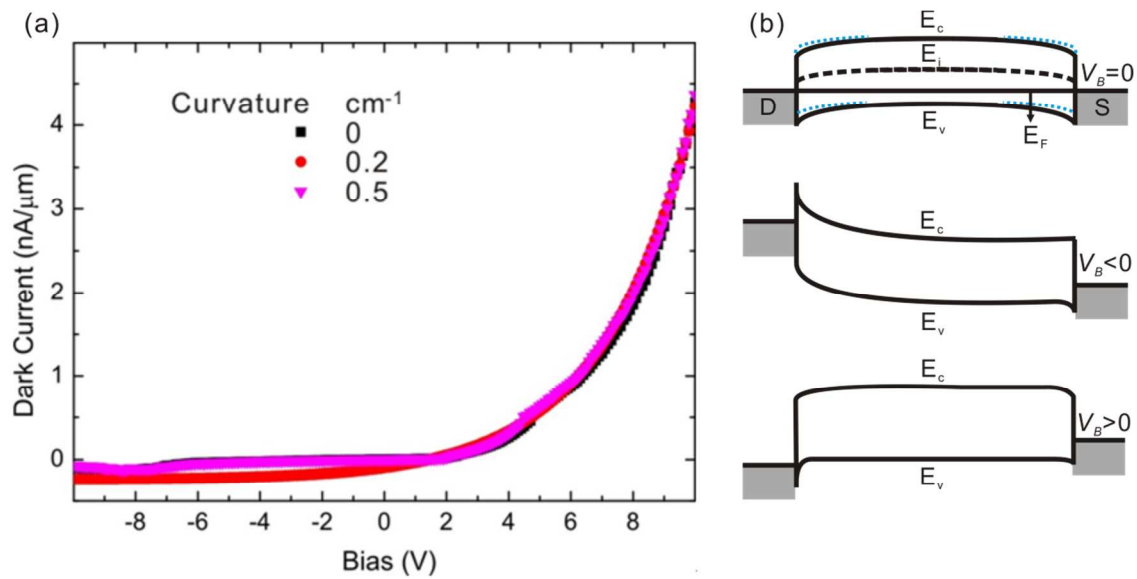


Figure S4. (a) Dark current versus bias (I-V) curves of Si-NMs with various bending curvatures (0, 0.2, 0.4, cm^{-1}). (b) Ideal band edge alignments of the constructed device in dark and under illumination when $V_B = 0, < 0$ and > 0 . E_F is the Fermi level, and E_C is the bottom of conduction band, E_V is the top of valence band.

To illustrate the inside mechanism of photo-response property of Si-NM-fiber photodetectors, **Figure S4b** shows band profiles of designed Si-NM-based device at source-drain biases (V_B) of 0 (upper), negative bias (middle), and positive bias (down) under illumination, respectively. The alignment of the Fermi level relative to the bandgap depends on many parameters. The simplest model assumes that the Schottky barrier is given by $\Phi_B = \Phi - \chi$, where Φ is the metal workfunction and χ is the semiconductor electron affinity, leading to a calculated electron barrier height in **Figure S4b** of 0.21 eV (electron affinity of Si is 4.05 eV and the work function of Ag is 4.26 eV). However, Si-NMs absorb light illumination and electron-hole pairs generate at surface, tuning doping level and then modulating Schottky barrier. More specifically, unlike conventional bulk semiconductor, Schottky barrier of ultra-thin semiconductor nanomembrane is far more sensitive to doping at the surface, i.e., surface doping which is sensitive to external stimuli for instance light illumination.¹ One possible reason is the depletion width, which depends exponentially on the doping density and thus changes with light illumination.² It means that when illuminated, the depletion width at nanoscale metal/semiconductor interfaces (including nanomembranes and nanowires) is reduced more than that in bulk material, as displayed as blue dotted line in the upper part of **Figure S4b**. Thus, the injected carriers significantly increase due to decrease of the depletion width and thus the larger current could be obtained. The fluctuation of the bias voltage V_B also has a remarkable influence

on the density of free electrons in the channel from metal electrodes. When a negative bias ($V_B < 0$) is applied to the drain contact, the band edge bends upward at the drain side, as displayed in middle part of **Figure S4b**. At low voltages, the electron barrier is too high for electron injection; as a result, the current is low. With increasing voltage, the barrier can be overcome by electrons while the respective injection becomes easy. However, the injection of holes at the source contact is still difficult either at low or high biases.³ Similar statement can be implanted into the device under a positive bias ($V_B > 0$), as shown in the down panel of **Figure S4b**.

References

- (1) Feng, P.; Mönch, I.; Huang, G. S.; Harazim, S.; Smith, E. J.; Mei, Y. F.; Schmidt, O. G. Local-Illuminated Ultrathin Silicon Nanomembranes with Photovoltaic Effect and Negative Transconductance. *Adv. Mater.* **2010**, *22*, 3667-3671.
- (2) Kamieniecki, E. Defect Specific Photoconductance: Carrier Recombination Through Surface and Other Extended Crystal Imperfections. *J. Appl. Phys.* **2012**, *112*, 063715.
- (3) Feng, P.; Mönch, I.; Huang, G. S.; Harazim, S.; Smith, E. J.; Mei, Y. F.; Schmidt, O. G. Local-Illuminated Ultrathin Silicon Nanomembranes with Photovoltaic Effect and Negative Transconductance. *Adv. Mater.* **2010**, *22*, 3667-3671.